Orbital state and magnetic properties of LiV2O4

Igor A. Nekrasov, Z. V. Pchelkina, Georg Keller, Thomas Pruschke, Karsten Held, Alexander Krimmel, Dieter Vollhardt, V. I. Anisimov

Angaben zur Veröffentlichung / Publication details:

Nekrasov, Igor A., Z. V. Pchelkina, Georg Keller, Thomas Pruschke, Karsten Held, Alexander Krimmel, Dieter Vollhardt, and V. I. Anisimov. 2003. "Orbital state and magnetic properties of LiV2O4." *Physical Review B* 67 (8): 085111. https://doi.org/10.1103/PhysRevB.67.085111.

Orbital state and magnetic properties of LiV_2O_4

I. A. Nekrasov,[1,2] Z. V. Pchelkina,[1,2,3] G. Keller,[2] Th. Pruschke,[2] K. Held,[4] A. Krimmel,[5] D. Vollhardt,[2] and V. I. Anisimov[1,2]
[1]*Institute of Metal Physics, Russian Academy of Sciences-Ural Division, 620219 Yekaterinburg GSP-170, Russia*
[2]*Theoretical Physics III, Center for Electronic Correlations and Magnetism, Institute for Physics, University of Augsburg, D-86135 Augsburg, Germany*
[3]*Department of Theoretical Physics and Applied Mathematics, Ural State Technical University, 620002 Yekaterinburg Mira 19, Russia*
[4]*Max Planck Institute for Solid State Research, Heisenbergstrasse 1, D-70569 Stuttgart, Germany*
[5]*Experimental Physics V, Center for Electronic Correlations and Magnetism, Institute for Physics, University of Augsburg, D-86135 Augsburg, Germany*

(Received 30 August 2002; revised manuscript received 11 November 2002; published 28 February 2003)

LiV_2O_4 is one of the most puzzling compounds among transition metal oxides because of its heavy-fermion-like behavior at low temperatures. In this paper we present results for the orbital state and magnetic properties of LiV_2O_4 obtained from a combination of density functional theory within the local density approximation and dynamical mean-field theory (DMFT). The DMFT equations are solved by quantum Monte Carlo simulations. The trigonal crystal field splits the V $3d$ orbitals such that the a_{1g} and e_g^{π} orbitals cross the Fermi level, with the former being slightly lower in energy and narrower in bandwidth. In this situation, the d-d Coulomb interaction leads to an almost localization of one electron per V ion in the a_{1g} orbital, while the e_g^{π} orbitals form relatively broad bands with 1/8 filling. The theoretical high-temperature paramagnetic susceptibility $\chi(T)$ follows a Curie-Weiss law with an effective paramagnetic moment $p_{\mathrm{eff}}=1.65$ in agreement with the experimental results.

DOI: 10.1103/PhysRevB.67.085111 PACS number(s): 71.27.+a, 71.10.Hf

I. INTRODUCTION

Heavy-fermion (HF) materials are typically intermetallic compounds containing Ce, U, or Yb atoms. They are characterized by extraordinarily strongly renormalized effective masses $m^* \approx 100-1000\ m_e$,[1–3] as inferred from the electronic specific heat coefficient $\gamma(T) \equiv C_e(T)/T$ at low temperature. They also show an apparent local moment paramagnetic behavior with a strongly enhanced spin susceptibility χ at low temperatures. The discovery by Kondo *et al.*[4] of the HF behavior in LiV_2O_4 with a Kondo or spin fluctuation temperature $T_K \sim 28$ K has significant importance, because this is the first d-electron system that shows HF characteristics. Kondo *et al.* reported a large electronic specific heat coefficient $\gamma \approx 0.42$ J/(mol K^2) at 1 K, which is much larger than those of other metallic transition metal compounds such as, e.g., $Y_{1-x}Sc_xMn_2$ [$\gamma \lesssim 0.2$ J/(mol K^2)][5] and $V_{2-y}O_3$ [$\gamma \lesssim 0.07$ J/(mol K^2)].[6] Also a crossover from the local moment to a renormalized Fermi-liquid behavior was observed with decreasing temperature. Recently Urano *et al.*[7] reported that the electrical resistivity ρ of single crystals exhibits a T^2 temperature dependence $\rho = \rho_0 + AT^2$ with an enormous A, which as in conventional HF systems scales with γ^2.[8] In the temperature range 50–1000 K the experimental magnetic susceptibility follows a Curie-Weiss law with a negative Curie-Weiss temperature, which indicates a weak antiferromagnetic (AF) V-V spin interaction (see later in the text). No magnetic ordering was observed down to 0.02 K.[4]

These unexpected phenomena entailed numerous experiments, which confirmed the HF behavior of LiV_2O_4 in a variety of physical quantities: Johnston *et al.*[9] carried out specific heat and thermal expansion measurements. Hayakawa *et al.*[10] investigated Metal-Insulator transition in $LiTi_{2-x}V_xO_4$ at $x \simeq 1$. Kondo *et al.*[11] described the synthesis, characterization and magnetic susceptibility versus temperature. Onoda *et al.*[12] explored spin fluctuations and transport in the spinel systems $Li_xMg_{1-x}V_2O_4$ and $Li_xZn_{1-x}V_2O_4$ through measurements of x-ray diffraction, electrical resistivity, thermoelectric power, magnetization, and nuclear magnetic resonance (NMR). The electron-spin resonance (ESR) and the magnetic susceptibility in pure and doped LiV_2O_4 were measured by Lohmann *et al.*[13] Photoemission studies of the hole doped Mott insulator $Li_{1-x}Zn_xV_2O_4$ were done by Fujimori *et al.*[14] A series of ^{7}Li-NMR experiments were carried out by Fujiwara *et al.*[15] for LiV_2O_4 and also for $Li_{1-x}Zn_xV_2O_4$.[16] The Knight shift, spin susceptibility and relaxation times were determined from ^{7}Li-NMR experiments by Mahajan *et al.*[17] Krimmel *et al.*[18] presented results for the magnetic relaxation of LiV_2O_4 obtained by means of quasielastic neutron scattering. Trinkl *et al.*[19] investigated spin-glass behavior in $Li_{1-x}Zn_xV_2O_4$. Urano *et al.*[7] experimentally observed results for $C(T)$, $\chi(T)$, resistivity $\rho(T)$ and Hall coefficient $R_H(T)$ for single crystal samples. Recently, Lee *et al.*[20] performed inelastic neutron scattering measurements and Fujiwara *et al.*[21] studied the spin dynamics under high pressure. A review of various experiments and theoretical research is collected in the work of Johnston.[22]

Let us summarize the experimental efforts concerning the measurements of the spin susceptibility $\chi(T)$. As mentioned before, a temperature dependent spin susceptibility $\chi(T)$ is observed in the temperature range from 50 to 1000 K, which fits well to the Curie-Weiss law[4,7,9–13,15–17,19,20,22–30] $\chi(T) = \chi_0 + C/(T-\theta)$. However, depending on the quality of samples and experimental techniques, the values of the Curie constant C obtained from fitting the experimental data are in the range from 0.329–0.468 cm^{3}K/mol.[17,26] More important and of direct physical importance is the value of the effective

paramagnetic moment p_{eff}, which is defined via the Curie constant as $p_{\mathrm{eff}}^2 := 3Ck_B/(N_A\mu_B^2)$. The extracted value p_{eff} lies in the range between 1.62 and 2.1.[20,29] The Curie-Weiss temperature obtained in those experiments is also slightly different and encompasses the interval $\theta = -20 \cdots -60$ K, which indicates a weak antiferromagnetic (AF) V-V spin interaction. If one further assumes that the effective spin value is $S=1/2$, an experimental estimation of the Landé factor $g^2 = p_{\mathrm{eff}}^2/[S(S+1)]$ leads to values between 1.87 and 2.23.[17,26]

From a theoretical point of view, LiV_2O_4 has been intensively studied by standard band structure calculations by various groups using different implementations of density functional theory[31] (DFT) within the local density approximation (LDA).[32] Anisimov *et al.*[33] investigated the possibility of localization of the *d*-states in LiV_2O_4 within the linearized muffin-tin orbitals (LMTO) basis[34] supplemented by the LDA+U method.[35] The electronic structure was furthermore studied by Eyert *et al.*[36] with the scalar-relativistic augmented spherical wave (ASW) basis,[37] while Matsuno *et al.*[38] used a full-potential, scalar-relativistic implementation[39] of the linear augmented plane wave (LAPW) approach[40] for the band structure calculation and furthermore applied a simple tight-binding (TB) model.[41] Singh *et al.*[42] also used the full potential LAPW (Refs. 43–45) for calculating the band structure and a TB-LMTO method[34] to analyze the band symmetry.

A relative comparison of LiV_2O_4 and lithium titanate ($LiTi_2O_4$) with original HF systems was done by Varma[46] to provide some qualitative understanding of these compounds. The two-band Hubbard model in the slave-boson mean-field approximation was applied to LiV_2O_4 by Kusunose *et al.*[47] to investigate the evolution of bands due to the Coulomb interactions. Hopkinson *et al.* presented a simple two-band model[48] and a *t-J* model with a strong Hund's coupling for the *d* electrons[49] to find evidence for a two-stage screening in LiV_2O_4. Fujimoto investigated the Hubbard chains network model on corner-sharing tetrahedra as a possible microscopic model for the HF behavior in LiV_2O_4.[50] The competition between the Kondo effect and frustrating exchange interactions in a Kondo-lattice model within a large-*N* approach for the spin liquid together with dynamical mean-field theory were studied by Burdin *et al.*[51]

Despite all this theoretical effort, there does not yet exist an undisputed microscopic explanation of the HF behavior of LiV_2O_4 at low temperatures. It has been attempted to explain the low-temperature properties of LiV_2O_4 by a mechanism analogous to one for systems with local moments on a pyrochlor lattice, which are frustrated with respect to the antiferromagnetic interactions. An attempt to provide a microscopic model based on material properties of LiV_2O_4, which does not evoke the idea of frustration was suggested by Anisimov *et al.*[33] Their basic idea is a separation of the electrons on partially filled t_{2g} orbitals into localized ones, forming local moments, and delocalized ones, producing a partially filled metallic band. The hybridization between those two subsets of electrons, as in *f*-electron materials, can give rise to heavy-fermion effects. However, in this work the conclusions were based on an LDA+U calculation,[35] which is essentially a static mean-field approximation and surely too crude to give a proper description of LiV_2O_4.

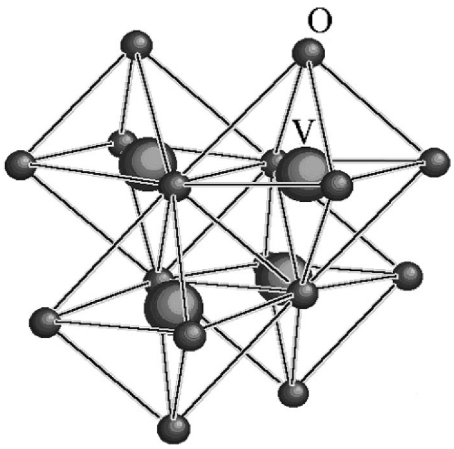

FIG. 1. The normal-spinel crystal structure of LiV_2O_4 is formed by the oxygen edge-shared octahedra with V atoms at the centers. V: large dark spheres; O: small dark spheres.

The present work reports on the investigation of the orbital state and the magnetic properties of LiV_2O_4 using the LDA+DMFT(QMC) approach. This material specific theory extracts informations about the noninteracting band structure from a DFT/LDA calculation, while treating the local Coulomb interactions via the dynamical mean-field theory (DMFT), which is a well-established nonperturbative approach to study localization effects in strongly correlated materials. The resulting DMFT equations are then solved by quantum Monte Carlo simulations. The main goal of this study is to further explore the idea of a separation of the *d* electrons in LiV_2O_4 into two subsets, localized and itinerant as proposed in Ref. 33. The rest of the paper is divided into two parts: In the first we discuss standard DFT/LDA results (Sec. II) and then present our LDA+DMFT(QMC) results in the second (Sec. III). A short summary concludes the paper.

II. LiV_2O_4: DFT/LDA RESULTS

A. Crystal structure and *d* orbital splitting

LiV_2O_4 has the fcc normal-spinel structure with nonsymmorphic space group $Fd3m$ and was first synthesized by Reuter and Jaskowsky in 1960.[52] The Li ions are tetrahedrally coordinated by oxygens, while the V sites are surrounded by a slightly distorted edge-shared octahedral array of oxygens (Fig. 1). The corresponding unit cell of the face-centered cubic lattice contains two LiV_2O_4 formula units (14 atoms) with four V atoms, which form a tetrahedron (Fig. 2). The LiV_2 substructure is the same as the $C15$ structure AB_2, where the local moments at the *B* sites are highly frustrated.[53] The observed lattice constant of LiV_2O_4 is 8.22672 Å at 4 K.[54] The eight oxygen atoms in the primitive cell are situated at the 32*e*-type sites, at positions which are determined by the internal-position parameter $x=0.2611$ in units of the lattice constant.

The total space group of the crystal is cubic but the local point group symmetry of the V ion crystallographic position

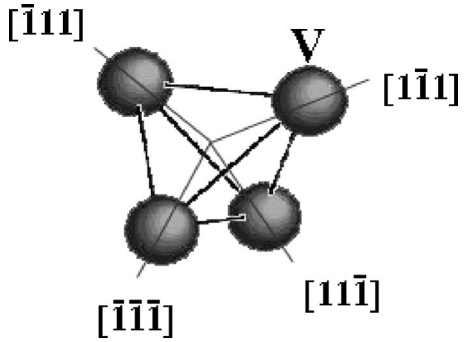

FIG. 2. Tetrahedron formed by four V atoms (large dark spheres) in the spinel unit cell and the trigonal axes for each V atom.

is trigonal D_{3d}. The different trigonal axes of every V atom in the unit cell are directed towards the center of the tetrahedron (Fig. 2). Since the formal oxidation state of V is noninteger $V^{3.5+}$ (configuration $d^{1.5}$) and the V ions are crystallographically equivalent, LiV_2O_4 must be metallic as it is observed.[52]

The octahedral crystal field at the V sites in the spinel structure splits the V $3d$ bands into three degenerate and partially filled t_{2g} bands and two empty e_g^σ bands. The Fermi level lies within the t_{2g} complex, thus the transport properties of LiV_2O_4 are solely associated with the t_{2g} bands. The trigonal symmetry of the V ions splits the cubic t_{2g} levels into one a_{1g} and two degenerate e_g^π levels (Fig. 3). However, this splitting is not large enough to separate the t_{2g} band into two subbands.[38]

B. DFT/LDA band structure

Based on DFT/LDA (Refs. 31,32) within the LMTO method,[34] we performed first-principle calculations of the electronic structure of LiV_2O_4. The radii of the muffin-tin spheres were $R_{Li}=2.00$ a.u., $R_V=2.05$ a.u., and $R_O=1.67$ a.u. The resulting densities of states (DOS) are shown in Figs. 4 and 5. In Fig. 4, there are three well-separated sets of bands: completely filled O-$2p$ bands, partially filled t_{2g} bands, and empty e_g^σ bands. The bands in the energy range from -8 eV to -3 eV originate mainly from O-$2p$ states

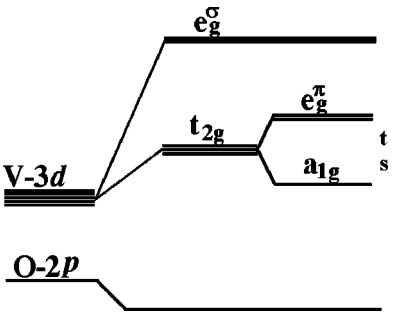

FIG. 3. Schematic picture of the electronic level distribution caused by the strong p-d hybridization in the trigonally distorted octahedral crystal field. The notations t_{2g} and e_g^σ correspond to the irreducible representations of the cubic O_h group, a_{1g} and e_g^π to the irreducible representations of the D_{3d} group.

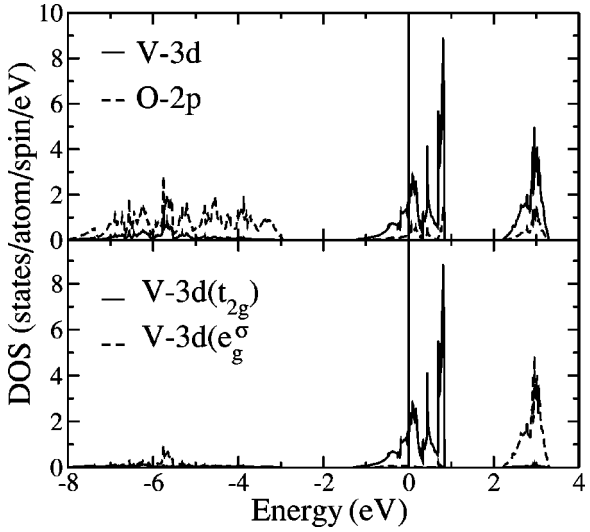

FIG. 4. DOS of LiV_2O_4 calculated with the LDA-LMTO method. Upper figure: V-$3d$ (full line) and O-$2p$ (dashed line) DOS; lower figure: partial V-$3d(t_{2g})$ (full line) and V-$3d(e_g^\sigma)$ (dashed line) DOS. The Fermi level corresponds to zero energy.

and have only small admixtures from V-$3d$ states. The upper two groups of bands, which extend from -1.0 to 0.8 eV and from 2.3 to 3.2 eV, are predominantly derived from the V-$3d$ states. Although additional small O-$2p$ contributions are apparent in this energy range, the p-d hybridization is much reduced compared to other early transition metal oxides.[55] Due to the crystal field of the slightly distorted octahedral coordination of the V atoms by the oxygen atoms, a clear separation of the $3d$ t_{2g} and e_g^σ groups of bands is visible in Fig. 4. Whereas the former states appear exclusively around the Fermi energy, the e_g^σ states prevail at higher energies. Contributions of the V $3d$ states to the oxygen-derived bands originate almost exclusively from the e_g^σ states, which form σ bonds and experience a strong overlap with the O-$2p$

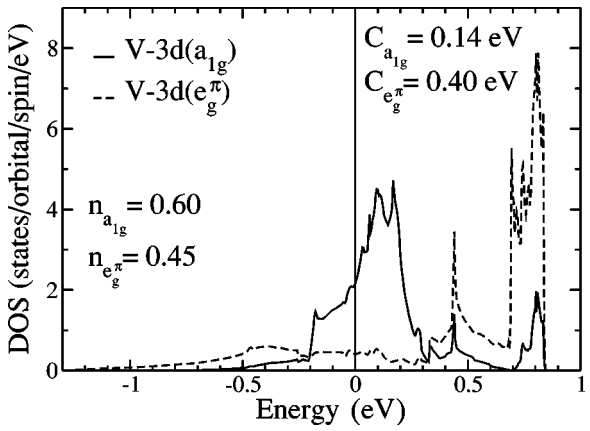

FIG. 5. Partial V-$3d(t_{2g})$ DOS of LiV_2O_4 calculated with the LDA-LMTO method: a_{1g} (full line) and e_g^π (dashed line) projected DOS. The center of gravity of the a_{1g} orbital is $c_{a_{1g}}=0.14$ eV; that of the e_g^π orbital is $c_{e_g^\pi}=0.40$ eV. The LDA-calculated occupancies of the a_{1g} and e_g^π orbitals, $n_{a_{1g}}=0.60$ and $n_{e_g^\pi}=0.45$, are nearly the same. The Fermi level corresponds to zero energy.

states. In contrast, the t_{2g} orbitals, which give rise to π bonds, yield only a negligible contribution in this energy range. In addition to p-d bonds, the t_{2g} states experience strong σ-type overlap with the t_{2g} orbitals at neighboring vanadium sites of the fcc sublattice. Hence, these d states take part in two different types of bonding, namely, σ-type V-V and π-type V-O bonding, which leads to two different bandwidths for t_{2g} and e_g^σ states. Since both the metal-metal and metal-oxygen bonds are mediated through the same orbital, a simple analysis of the partial DOS would not allow to distinguish the different roles played by the t_{2g} orbitals. Eyert *et al.*[36] used a local coordinate system with the Z axis along the trigonal direction (111) pointing towards the center of the tetrahedron formed by V ions (see Fig. 2) and plotted the V $d_{3z^2-r^2}$, $d_{xz}+d_{yz}$, and $d_{x^2-y^2}+d_{xy}$ partial DOS. While $d_{3z^2-r^2}$ orbitals are of pure t_{2g} character, the other four orbitals comprise a mixture of t_{2g} and e_g^σ states. We have calculated the partial DOS for a_{1g} and e_g^π orbitals, using the irreducible representations of the D_{3d} group according to Terakura *et al.*[56] with the following linear combinations of the t_{2g} cubic harmonics: the a_{1g} orbital is given by $(xy+xz+yz)/\sqrt{3}$ and the two e_g^π orbitals by $(zx-yz)/\sqrt{2}$ and $(yz+zx-2xy)/\sqrt{6}$. These three particular linear combinations are valid if the coordinate axes X, Y, and Z are directed along V-O bonds. If the Z direction is chosen along one of the trigonal axes described above, then the a_{1g} orbital is the $3z^2-r^2$ orbital in the local coordinate system.

The projected partial LDA DOS of the a_{1g} and the e_g^π orbitals are shown in Fig. 5. The bandwidth of the a_{1g} orbital $W_{a_{1g}}=1.35$ eV is almost a factor of 2 smaller than the e_g^π bandwidth $W_{e_g^\pi}=2.05$ eV. Nonetheless, we found within LDA for all three t_{2g} derived orbitals nearly the same occupancies: $n_{a_{1g}}=0.60$ and $n_{e_g^\pi}=0.45$. Almost all spectral weight of the a_{1g} orbital is concentrated around the Fermi level in the region from -0.2 to 0.3 eV. In contrast to the a_{1g} orbital the e_g^π DOS is flat at the Fermi level. The largest part of the spectral weight of the e_g^π orbitals is situated in the interval from 0.3 to 0.85 eV. Despite such a different spectral weight the a_{1g} and e_g^π bands are not completely separated in energy. However, there is a significant difference in the centers of gravity calculated from the corresponding partial DOS, which can be interpreted as a measure for the trigonal splitting of the t_{2g} states.

The trigonal splitting is much smaller than the bandwidth but has a great importance for the understanding of the physics of the LiV_2O_4 system in the presence of strong Coulomb interaction. The value and the sign of the trigonal splitting will determine the orbital in which the V 3d electrons should be localized when a strong Coulomb interaction, which is larger than the bandwidth, is taken into account.[33] We found that this trigonal splitting value is very sensitive to the accuracy of the band structure calculations. In order to increase the accuracy, the overlap between atomic spheres in our LMTO calculation was set to zero and more empty spheres were introduced. For the following we *define* the trigonal splitting of the t_{2g} states as the difference of the centers of gravity of the a_{1g} and the e_g^π projected DOS. We find that the a_{1g} center of gravity is 0.26 eV lower than that of the e_g^π band ($c_{a_{1g}}=0.14$ eV, $c_{e_g^\pi}=0.40$ eV; see Fig. 5). One can thus conclude from our LDA calculations that the a_{1g} orbital is more favorable for the localization of electrons.

The effective mass m^* is known to be a measure for the Coulomb correlations and can be obtained from the electronic specific heat coefficient γ at low temperatures. From the LDA-calculated electronic specific heat coefficient γ^{LDA}, one can infer the ratio of the effective mass to the band mass $m^*/m_b=\gamma/\gamma^{\mathrm{LDA}}$. Here, the former is related to the LDA DOS at the Fermi level via $\gamma^{\mathrm{LDA}}=\pi^2 k_B^2 N_A D(E_F)/3$, and γ is the experimental value of the electronic specific heat coefficient taken from.[4] For LiV_2O_4 we found $m^*/m_b\approx 25.8$, which is in good agreement with previous results.[38] Such a huge enhancement of the quasiparticle mass m^* is a strong evidence that Coulomb correlations are important in LiV_2O_4 and have to be taken into account in order to describe the physics of this system.

III. A MICROSCOPIC THEORY FOR LiV_2O_4

A. LDA+DMFT(QMC) scheme

Based on the $d=\infty$ limit,[57] the dynamical mean-field theory (DMFT) (Refs. 58–60) was developed as a nonperturbative approach to describe strongly correlated electron systems. It permits the calculation of electronic spectra for systems with local electronic Coulomb correlations. The LDA+DMFT approach is a merger of the DFT/LDA and the DMFT techniques.[61,62] It combines the strength of the DFT/LDA, viz describing the weakly correlated part of the *ab initio* Hamiltonian, i.e., electrons in s and p orbitals and the long-range part of the Coulomb interaction, with the ability of the DMFT to treat electronic correlations induced by the local Coulomb interaction. In this paper we will only briefly discuss the relevant parts of the LDA+DMFT approach and refer the reader to a recent report by Held *et al.*[63] for more details.

For a given material, one can extract a LDA Hamiltonian $\hat{H}^0_{\mathrm{LDA}}$ and supplement the local Coulomb interactions

$$\hat{H}=\hat{H}^0_{\mathrm{LDA}}+U\sum_m\sum_i \hat{n}_{im\uparrow}\hat{n}_{im\downarrow} + \sum_i\sum_{m\neq m'}\sum_{\sigma\sigma'}(U'-\delta_{\sigma\sigma'}J)\hat{n}_{im\sigma}\hat{n}_{im'\sigma'}. \quad (1)$$

Here, the index i enumerates the V sites, m denotes the individual t_{2g} orbitals, and σ the spin. H^0_{LDA} is a one-particle Hamiltonian generated from the LDA band structure with an averaged Coulomb interaction subtracted to avoid a double counting of the Coulomnb interaction.[61] U is the local intraorbital Coulomb repulsion and J the exchange interaction. The local interorbital Coulomb repulsion U' is then fixed by rotational invariance: $U'=U-2J$. The actual values for U and U' can be obtained from an averaged Coulomb parameter $\bar{U}$ and Hund's exchange J, which can be calculated with LDA. The quantity $\bar{U}$ is related to the Coulomb parameters U and U' via

$$\bar{U} = \frac{U + (N_{\rm orb}-1)U' + (N_{\rm orb}-1)(U'-J)}{2N_{\rm orb}-1}, \qquad (2)$$

where $N_{\rm orb}$ is the number of interacting orbitals ($N_{\rm orb}=3$ in our case). Since U and U' are not independent, the two values $\bar{U}$ and J are sufficient to determine U from this relation.[63,69]

The DMFT maps the lattice problem (1) onto an effective, self-consistent impurity problem. A reliable method to solve this (multiband) quantum impurity problem is provided by quantum Monte Carlo (QMC) simulations,[64] which are combined with the maximum entropy method[65] for the calculation of spectral functions from the imaginary time QMC data. This technique has been applied to calculate properties of several transition metal oxides.[66,68,70]

A computationally important simplification is due to the fact that in cubic spinel the t_{2g} states do not mix with the e_g^σ states. In this particular case the self-energy matrix $\Sigma_{m\sigma}(z)$ is diagonal with respect to the orbital and spin indices. Under this condition the Green functions $G_{m\sigma}(z)$ of the lattice problem can be expressed in the DMFT as Hilbert transform of the noninteracting DOS $N_m^0(\epsilon)$,

$$G_{m\sigma}(z) = \int d\epsilon \frac{N_m^0(\epsilon)}{z - \mu_B B\sigma - \Sigma_{m\sigma}(z) - \epsilon}. \qquad (3)$$

This procedure avoids the rather cumbersome and problematic k integration over the Brillouin zone by the analytical tetrahedron method.[71] The LDA DOS $N_m^{(0)}(\epsilon)$ for different orbitals (different m) of the $3d$ t_{2g} states in LiV_2O_4 is displayed in Fig. 5.

A particularly interesting quantity for LiV_2O_4 is the magnetic susceptibility $\chi(T)$. In order to calculate $\chi(T)$ we use the definition $\chi(T)=\lim_{B\to 0} M(T)/B$, where $M(T)$ is the magnetization due to the applied magnetic field B. Obviously, $M(T)$ can be obtained directly from the QMC data via

$$M(T) = \mu_B \sum_{m=1}^{N_{\rm orb}} (\langle n_{m\uparrow}\rangle - \langle n_{m\downarrow}\rangle) \qquad (4)$$

and

$$\langle n_{m\sigma}\rangle = G_{m\sigma}(\tau = 0^+). \qquad (5)$$

Since QMC results are subject to both statistical and systematic errors, a direct evaluation of $M(T)/B$ for small B will inevitably lead to unpredictable scattering of the results for $\chi(T)$. To avoid these problems, we perform calculations for $M(T,B)$ for a series of small fields B and extract $\chi(T)$ from a least-squares fit as the slope of $M(T,B)$ as $B\to 0$.

B. Single-particle properties

The DMFT calculations are based on the DFT/LDA-DOS $N_m^0(\epsilon)$ for the a_{1g} and e_g^π orbitals presented in Fig. 5. The total number of electrons in these three orbitals was fixed to $n=1.5$, in accordance with the $+3.5$ valency of V ions in LiV_2O_4. The d-d Coulomb interaction parameter $\bar{U}=3.0$ eV and exchange Coulomb interaction parameter $J=0.8$ eV were calculated[33] by the constrained LDA method.[72] The temperature used in our QMC simulations was approximately 750 K. While the scheme in principle poses no restrictions on the temperature values, the QMC code used presently limits our calculations to these rather high temperatures because of computing power limitations.[66]

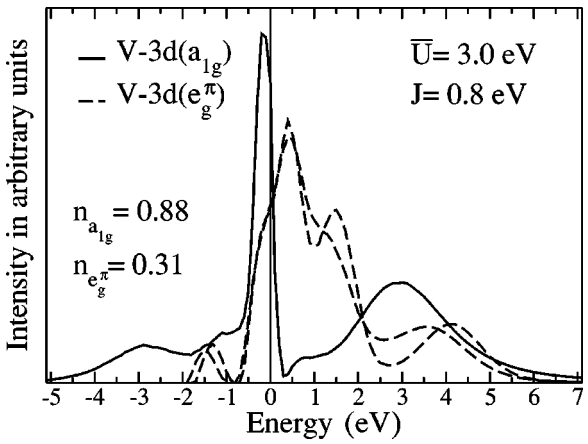

FIG. 6. Partial a_{1g} and e_g^π DOS for LiV_2O_4 calculated with LDA+DMFT(QMC) for $\bar{U}=3.0$ eV and $J=0.8$ eV. The noninteracting DOS $N_m^0(\epsilon)$ used in the LDA+DMFT calculations are presented in Fig. 5. The LDA+DMFT(QMC) occupancies of the a_{1g} and e_g^π orbitals are $n_{a_{1g}}=0.88$ and $n_{e_g^\pi}=0.31$. The Fermi level corresponds to zero energy.

The partial DOS of a_{1g} and e_g^π orbitals obtained from the analytical continuation of the QMC results are shown in Fig. 6. In comparison with the non-interacting case (see Fig. 7), a considerable transfer of spectral weight has taken place, especially the a_{1g} orbital appears to be strongly renormalized by Coulomb interactions. Furthermore, in contrast to the LDA results, where the occupation of the a_{1g} and e_g^π orbitals is roughly the same, the DMFT yields $n_{a_{1g}}\approx 0.9$ and $n_{e_g^\pi}$

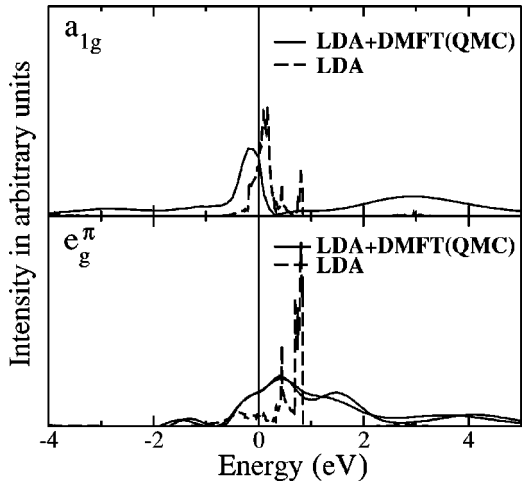

FIG. 7. LDA+DMFT(QMC) calculated DOS for LiV_2O_4 (solid line; $\bar{U}=3.0$ eV and $J=0.8$ eV) in comparison with noninteracting LDA a_{1g} and e_g^π DOS (dashed line). Please note that for a more convenient comparison the LDA+DMFT(QMC) DOS were magnified in intensity by a factor of 5. The Fermi level corresponds to zero energy.

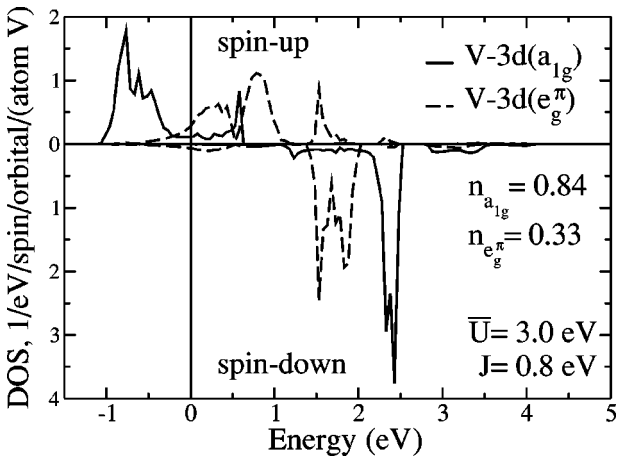

FIG. 8. LDA+U results (Ref. 67) for spin-resolved partial a_{1g} and e_g^π DOS for LiV_2O_4 ($\bar{U}=3.0$ eV and $J=0.8$ eV). The LDA+U occupancies of the a_{1g} and e_g^π orbitals are $n_{a_{1g}}=0.84$ and $n_{e_g^\pi}=0.33$. The Fermi level corresponds to zero energy.

≈ 0.3. These numbers clearly demonstrate that one electron is nearly localized in the a_{1g} orbital, while the e_g^π states remain weakly correlated and metallic with a filling close to 1/8. Nevertheless, the e_g^π orbitals are remarkably broadened by Coulomb interactions in comparison with the LDA picture (Fig. 7). Slight differences between the two degenerate e_g^π orbitals originate from the statistical nature of the QMC method and the following analytical continuation with MEM.

Earlier, correlation effectcs in the electronic structure of LiV_2O_4 were taken into account by the LDA+U method.[33] The main result of this calculation was the localization of one V $3d$ electron per V ion in the a_{1g} orbital ($n_{a_{1g}}=0.84$). Since this calculation[33] was based on the LDA+U method, i.e., a static Hartree theory, the localization of the a_{1g} orbital could only be achieved by imposing an *artificial* antiferromagnetic order. It is obvious, that our present DMFT calculation substantially improves on this former calculation in that it is correctly done in the paramagnetic state and does not require any further manipulations. The magnetic ordering and static mean-field approximation lead to the larger energy splitting of the a_{1g} and e_g^π peaks in partial DOSes (Fig. 8) and, hence, stronger localization of the a_{1g} orbital compared with paramagnetic DMFT calculations (Fig. 6).

To discuss the origin of the structures in the DOS of Fig. 6, it is helpful to look at the spectrum of the atomic Hamiltonian and the corresponding positions of the one-particle excitations. The states corresponding to atomic occupancies up to two electrons are listed in Table I together with their energies. Since the Hubbard U is large and we have to accommodate 1.5 electrons, with one electron in the a_{1g} orbital, the ground state has to be a suitable mixture of two states, which both have a singly occupied a_{1g} orbital, but differ in the occupancy of the e_g^π orbitals. The inspection of all possibilities in Table I leaves only $|\sigma\rangle|0\rangle|0\rangle$, $|\sigma\rangle|\sigma\rangle|0\rangle$ and $|\sigma\rangle|0\rangle|\sigma\rangle$ as candidates. In order for these three to be (nearly) degenerate, $\epsilon_{a_{1g}}+\Delta\epsilon+U'-J=0$ or $\epsilon_{a_{1g}}=-U'+J-\Delta\epsilon$. Inserting the numbers for U' and J and the LDA value for $\Delta\epsilon$ leads to $\epsilon_{a_{1g}}\approx -3.1$ eV. The possible one-particle excitations with respect to this ground state configuration and their energies can now be constructed easily, leading to the results in Table II. It is important to note that the single-particle excitations of the a_{1g} orbital with $\omega_0<0$ have two distinct contributions, namely one of the usual type ''singly occupied $\rightarrow$ unoccupied,'' and a second that actually involves a doubly occupied state build of a mixture of a_{1g} and e_g^π states, i.e., a mixed-valent state. The energy of this latter excitation is given directly by the trigonal splitting, i.e., this feature can also serve as a means to extract this number from photoemission experiments.

TABLE I. Eigenstates and eigenenergies of the atomic Hamiltonian for total occupations less or equal to 2. $\epsilon_{a_{1g}}$ denotes the one particle energy of the a_{1g} orbital and $\Delta\epsilon\approx 0.26$ eV the trigonal splitting between a_{1g} and e_g^π orbitals.

a_{1g}	e_g^1	e_g^2	Energy
$\|0\rangle$	$\|0\rangle$	$\|0\rangle$	0
$\|\sigma\rangle$	$\|0\rangle$	$\|0\rangle$	$\epsilon_{a_{1g}}$
$\|0\rangle$	$\|\sigma\rangle$	$\|0\rangle$	$\epsilon_{a_{1g}}+\Delta\epsilon$
$\|0\rangle$	$\|0\rangle$	$\|\sigma\rangle$	$\epsilon_{a_{1g}}+\Delta\epsilon$
$\|2\rangle$	$\|0\rangle$	$\|0\rangle$	$2\epsilon_{a_{1g}}+U$
$\|\sigma\rangle$	$\|\sigma'\rangle$	$\|0\rangle$	$2\epsilon_{a_{1g}}+\Delta\epsilon+U'-J\delta_{\sigma\sigma'}$
$\|\sigma\rangle$	$\|0\rangle$	$\|\sigma'\rangle$	$2\epsilon_{a_{1g}}+\Delta\epsilon+U'-J\delta_{\sigma\sigma'}$
$\|0\rangle$	$\|2\rangle$	$\|0\rangle$	$2\epsilon_{a_{1g}}+2\Delta\epsilon+U$
$\|0\rangle$	$\|0\rangle$	$\|2\rangle$	$2\epsilon_{a_{1g}}+2\Delta\epsilon+U$
$\|0\rangle$	$\|\sigma\rangle$	$\|\sigma'\rangle$	$2\epsilon_{a_{1g}}+2\Delta\epsilon+U'-J\delta_{\sigma\sigma'}$

That the excitations listed in Table II directly map to the peaks in the DOS Fig. 6 can be shown by using another technique to solve the DMFT equations, namely resolvent perturbation theory and NCA (see, e.g., Ref. 69). This approach allows for a direct identification of different excitation channels (i.e., different initial particle numbers) *and* a distinction between a_{1g} and e_g^π states. The result is shown in Fig. 9, where the black lines denote a_{1g} and the gray ones e_g^π single-particle excitations. Full lines stand for a singly occu-

TABLE II. Single-particle excitations for the atomic model filled with 1.5 electrons. For spin-degenerate processes only one representative is listed.

a_{1g} orbital	
Excitation process	Excitation energy ω_0
$\|\sigma\rangle\|0\rangle\|0\rangle\rightarrow\|0\rangle\|0\rangle\|0\rangle$	$\epsilon_{a_{1g}}$
$\|\sigma\rangle\|\sigma\rangle\|0\rangle\rightarrow\|0\rangle\|\sigma\rangle\|0\rangle$	$-\Delta\epsilon$
$\|\sigma\rangle\|0\rangle\|0\rangle\rightarrow\|2\rangle\|0\rangle\|0\rangle$	$\epsilon_{a_{1g}}+U$
e_g^π orbitals	
Excitation process	Excitation energy ω_0
$\|\sigma\rangle\|0\rangle\|0\rangle\rightarrow\|\sigma\rangle\|\sigma\rangle\|0\rangle$	0
$\|\sigma\rangle\|\sigma\rangle\|0\rangle\rightarrow\|\sigma\rangle\|0\rangle\|0\rangle$	0
$\|\bar{\sigma}\rangle\|0\rangle\|0\rangle\rightarrow\|\bar{\sigma}\rangle\|\sigma\rangle\|0\rangle$	J

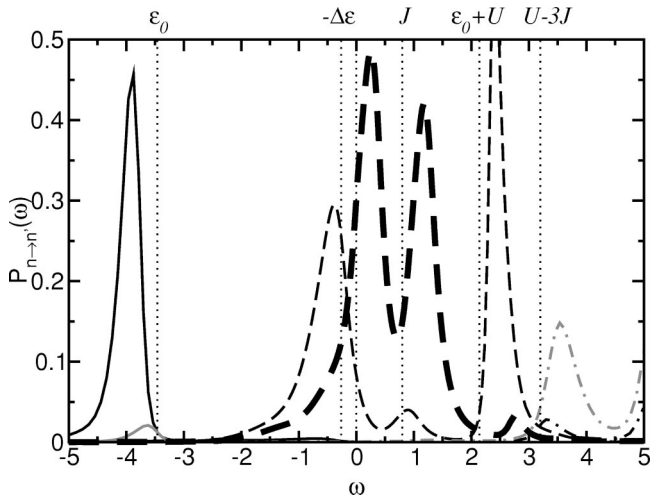

FIG. 9. One-particle DOS separated into different contributions. Black (thick) lines denote a_{1g} (e_g^π) single-particle excitations. Full (dashed) lines stand for a singly occupied (doubly occupied) initial state, dot-dashed lines for a triply occupied initial state. The dotted vertical lines show the positions of the excitations listed in Table II.

pied initial state, dashed lines for a doubly occupied initial state and dot-dashed lines for triply occupied initial state. Each of the dominant peaks correspond to one of the transitions listed in Table II. For clarity, the different excitation energies are marked by dotted vertical lines. Apparently, all peaks in Fig. 6 have their counterparts in Fig. 9, explaining them as *simply due to the atomic multiplet structure*. The shifts are typical renormalizations occurring in quantum impurity models. Especially the sharp peak at $\omega \approx -0.25$ eV in the a_{1g} DOS is part of the lower Hubbard band, i.e., the Fermi energy is located at the upper edge of the lower Hubbard band, leading to the observed filling close to 1. These explanations show that *no* Kondo resonances are seen in the LDA+DMFT(QMC) spectra at these elevated temperatures, consistent with experiment. Note also that the structures in the e_g^π band around $\omega \approx -1.5$ eV are related to corresponding features in the LDA e_g^π band located roughly 1.5 eV below the main structure at 0.75 eV (see Fig. 6). The double peak structure at $\omega > 0$, on the other hand, consists of two different processes with excitation energies $\omega_0 = 0$ and $\omega_0 = J$, respectively. Finally, the peak around $\omega = 4$ eV in the e_g^π DOS can be identified as an excitation into a triply occupied state $|\sigma\rangle|\sigma\rangle\sigma\rangle$ with energy $U-3J$.

The orbital occupation, which confirms the earlier conjecture based on the LDA+U approach,[33] can be readily understood from the previous analysis of the LDA band structure. There we found that the center of mass of the a_{1g} orbital is 0.26 eV lower than the corresponding value for the e_g^π orbitals. In the absence of Coulomb correlations the bandwidth is significantly larger than this energy difference, i.e., this splitting does not have any significant effect. However, with a Coulomb interaction $\bar{U} = 3.0$ eV, which is significantly larger than the kinetic energy term (bandwidth $W \approx 2$ eV), this small difference in connection with the smaller bandwidth of the a_{1g} orbitals will favor a localization of the electrons in the a_{1g} orbital for energetic reasons.

C. Paramagnetic susceptibility: Competition of two exchange processes

The LDA+DMFT(QMC) result that roughly one electron is localized in the a_{1g} orbital has several immediate consequences, which can be tested with experimental findings. A rather direct consequence is that the electron localized on the a_{1g} orbital leads to a local moment corresponding to $S = 1/2$ per vanadium atom and thus a Curie-like susceptibility, consistent with experiment. The remaining 0.5 electrons per V ion in the metallic e_g band will lead to a small and temperature independent Pauli contribution to the susceptibility.

From an experimental point of view, the magnetic properties of LiV_2O_4 pose several puzzles. LiV_2O_4 exhibits a paramagnetic Curie-Weiss susceptibility[4,7,9–13,15–17,19,20,22–30] $\chi(T) = C/(T-\theta) + \chi_0$ in the temperature range 50–1000 K. The best fit to the experimental data is obtained under the assumption that the magnetic susceptibility $\chi(T)$ is the sum of a Curie-Weiss and a T-independent part χ_0, which contains Pauli paramagnetic, core diamagnetic and orbital Van Vleck contributions to the total susceptibility.[17] If all V-3d electrons (1.5 per V ion) would equally contribute to the formation of a local moment, one would expect a mixture of $S=1$ and $S=1/2$ vanadium ions and consequently an effective paramagnetic moment 2.34. If only one localized electron in the a_{1g} orbital contributes to the Curie constant the effective paramagnetic moment is 1.73. However, the experimentally observed values of the Curie constants, as discussed above, in general are close to the latter value of the effective paramagnetic moment or slightly larger. Under the assumption that the local spin S is exactly 1/2 one gets a slightly enhanced g factor from experiment. Whereas the negative Curie-Weiss temperature in the range $\theta = -20 \cdots -60$ K indicates antiferromagnetic interactions between local $S=1/2$ moments, the large g value points towards ferromagnetic interactions between local moments and conduction electrons.[22,30]

A similar ambiguity is revealed by the results of ^{7}Li NMR measurements. The spin-lattice relaxation rate $1/T_1(T)$ shows a broad maximum around 30–50 K and becomes almost temperature independent above 400 K. The high temperature data ($T \geqslant 50$ K) have been interpreted either as an indication of localized magnetic moments[17] or, on the contrary, as characteristics of an itinerant electron system close to a ferromagnetic instability.[15]

The debate on the relevant magnetic interactions was continued after the spin fluctuation spectrum of LiV_2O_4 was determined by means of quasielastic neutron scattering.[18] These neutron data showed a transition from ferromagnetic correlations at elevated temperatures ($T \geqslant 40$ K) to antiferromagnetic spin fluctuations with a wave vector $q \approx 0.7$ Å^{-1} at low temperatures ($T \leqslant 40$ K), as shown in Fig. 10. However, a subsequent inelastic neutron scattering study on LiV_2O_4 reported the continuous evolution of antiferromagnetic fluctuations out of a high-temperature paramagnetic state without indications of ferromagnetic interactions at elevated temperatures.[20]

In order to clarify these inconsistencies, most recently, a polarized neutron scattering study on a set of LiV_2O_4

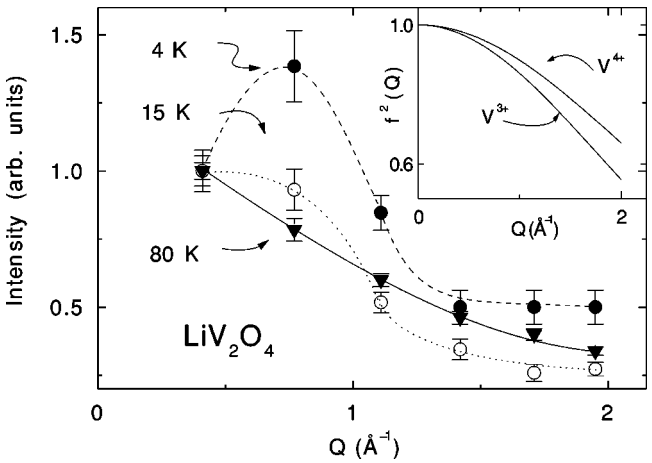

FIG. 10. Q dependence of the energy-integrated quasielastic scattering intensity of LiV_2O_4 at 4, 15, and 80 K. For comparison, the inset shows the Q dependence according to the square of the neutron magnetic form factor of the two vanadium configurations possible in LiV_2O_4. At elevated temperatures, the much stronger reduction of the scattering intensity upon increasing Q points towards ferromagnetic spin correlations. The maximum around $Q=0.7$ Å^{-1} at 4 K indicates antiferromagnetic fluctuations. Dashed or dotted lines are guides to the eye only (taken from Ref. 18).

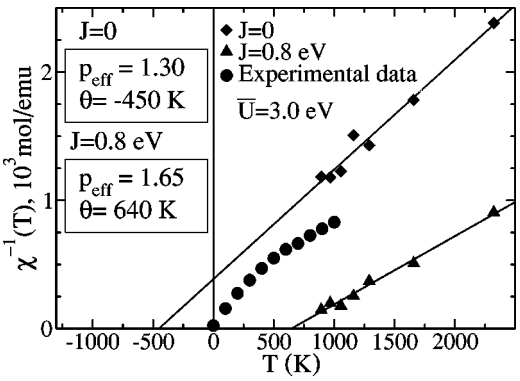

FIG. 11. Inverse Curie-Weiss spin susceptibility $\chi^{-1}(T)$ for LiV_2O_4 obtained by LDA+DMFT(QMC) calculation at $\bar{U}=3.0$ eV, $J=0$ (diamonds) and $J=0.8$ eV (triangles), in comparison to experimental data (Ref. 17) (circles). For (i) $J=0$ the Curie-Weiss constant is $\theta\approx-450$ K and the effective paramagnetic moment is $p_{\text{eff}}=1.30$; for (ii) $J=0.8$ eV we obtain $\theta\approx640$ K and $p_{\text{eff}}=1.65$. Solid lines are least squares fits to the LDA+DMFT(QMC) data.

samples has been performed.[76] Full three-directional polarization analysis allows for an unambiguous separation of the nuclear, magnetic and spin incoherent cross section, respectively. The measured magnetic cross section has been fitted and the corresponding real-space spin correlations extracted by employing the reverse Monte Carlo method. The data show a temperature induced cross-over from purely ferromagnetic next nearest neighbor spin correlations at high temperatures ($T\geqslant40$ K) to a coexistence of ferromagnetic (nearest neighbor) and antiferromagnetic (second nearest neighbor) correlations at low temperatures. The corresponding oscillatory behavior of the real-space spin correlations at low temperature can be described purely phenomenologically assuming a Ruderman–Kittel–Kasuya–Yosida-(RKKY-) type interaction with $S(S+1)=0.2$ and $k_F=0.45$ Å^{-1} for a simple parabolic band.[76] It has to be noticed that a value of 0.2 for $S(S+1)$ is much less than expected. This is due to the fact that these measurements were performed in a restricted energy transfer range of $hw<4$ meV. In turn, it can be concluded that a significant part of the spectral weight is beyond 4 meV. Due to the limited accessible energy transfer range so far, the spin correlations as determined on the basis of reverse Monte Carlo simulations definitively overemphasize the ferromagnetic contribution at low temperatures. In fact, there are indications of two different magnetic components corresponding to a ferromagnetic and an antiferromagnetic contribution, respectively. Their specific temperature dependencies give rise to a change from predominantly ferromagnetic correlations at high temperatures to predominantly antiferromagnetic correlations at low temperature. Let us estimate the band filling *per vanadium ion* that this particular value for k_F corresponds to. For a parabolic band we have

$$\frac{N_e}{N_{\text{sites}}}=n=\frac{1}{N_{\text{sites}}}\sum_{k<k_F,\sigma}=2\left(\frac{a}{2\pi}\right)^3\frac{4\pi k_F^3}{3},$$

where $a=8.227$ Å is the lattice constant. For $k_F=0.45$ Å^{-1} we obtain $n\approx1.714$ per cubic unit cell, i.e., a conduction band filling of 0.43 per vanadium ion, since there are four Vanadium ions per unit cell. Note that this value perfectly coincides with the filling of the e_g^π band as obtained within our LDA/DMFT calculation, thus giving further experimental confirmation of our proposed picture of a separation of the vanadium d states into a strongly correlated a_{1g} orbital with one localized electron and weakly localized e_g^π orbitals which form a metallic band filled with ≈0.5 electrons.

The evolution of antiferromagnetic spin correlations with $q\approx0.7$ Å^{-1} at low temperatures is now experimentally well established. However, the temperature-induced cross-over from ferromagnetic to RKKY-like spin correlations is still unclear at present.

We performed LDA+DMFT(QMC) calculations of the high-temperature magnetic susceptibility for a set of different inverse temperatures $\beta=5$, 7, 9, 10, 11, 12, 13 eV^{-1} and magnetic fields $B=0.005$, 0.01, 0.02 eV. The results are shown as triangles and diamonds for a Hund's exchange coupling $J=0.8$ eV and $J=0$, correspondingly, in Fig. 11 together with a fit to a Curie-Weiss law[73,74]

$$\chi(T)=N_A\frac{\mu_B^2p_{\text{eff}}^2}{3k_B(T-\theta)}.$$

The resulting value of the Curie-Weiss temperature is $\theta\approx640$ K for $J=0.8$ eV, the fitted Curie-Weiss constant C gives an effective magnetic moment $p_{\text{eff}}^2=g^2S(S+1)=2.71$, which corresponds to an effective paramagnetic moment $p_{\text{eff}}=1.65$. The deviation from $p_{\text{eff}}=1.73$ for a spin $S=1/2$ can be accounted for if one recalls that the occupancy of the a_{1g} orbital is not exactly 1 but 0.88. Such a reduced

occupancy should ideally lead to a decrease of p_{eff} from 1.73 to 1.52. The slightly larger (calculated) value $p_{\text{eff}}=1.65$ is due to contributions from the e_g states. For the calculation with $J=0$, where a_{1g} and e_g orbitals do not couple via a local exchange interaction the value of the effective paramagnetic moment is 1.3, which agrees with the expectations if one takes into account that for $J=0$ the occupancy of the a_{1g} orbital is 0.75, and hence $p_{\text{eff}}=1.73\times 0.75=1.3$.

While our value of p_{eff} is in good agreement with known experimental data, the large ferromagnetic Curie-Weiss temperature of about 640 K is in contrast with experiment. A similar result was obtained by Anisimov *et al.*,[33] where a rather strong effective ferromagnetic intersite exchange parameter $J_{\text{dex}}=530$ K (which is the sum of direct and double exchanges) was obtained. A ferromagnetic exchange coupling between local moments in LiV_2O_4 can be readily understood in the double exchange picture. The presence of two types of *d* electrons, localized ones forming local moments and delocalized ones producing a partially filled, relatively broad band, is a necessary ingredient for the double exchange mechanism, resulting in a strong ferromagnetic coupling between local moments. This requirement is fulfilled in the case of LiV_2O_4 with one electron localized in the a_{1g} orbital and a 1/8 filled broad e_g^{π} band.

A second important condition for the double exchange mechanism is Hund's intra-atomic exchange, i.e., the ferromagnetic exchange interaction between electrons within the t_{2g} states. If one switches off this intra-atomic exchange interaction, the double exchange mechanism will be switched off, too. This becomes apparent from the result of our calculations for $\chi^{-1}(T)$ with Hund's exchange *J* equal to zero (see Fig. 11, diamonds). Again, we obtain a Curie-Weiss-like behavior with an $p_{\text{eff}}=1.3$. This time, however, the Curie-Weiss temperature $\theta_{\text{dir}}\approx -450$ K is *negative*, i.e., pointing to an effective antiferromagnetic exchange. In the absence of intra-atomic exchange and a_{1g}-e_g^{π} hybridization, the only contribution to an exchange coupling can arise from the direct hybridization between the a_{1g} electrons. Obviously, this will result in the observed antiferromagnetic exchange coupling.

These results clearly show that, neglecting the a_{1g}-e_g^{π} hybridization, one has to expect a subtle competition in LiV_2O_4 between *antiferromagnetic* direct exchange resulting from the a_{1g}-a_{1g} hybridization and *ferromagnetic* double exchange from the e_g^{π}-e_g^{π} hybridization. Obviously, for the present set of Coulomb parameters the ferromagnetic contribution wins in our DMFT calculations. Note, that this result is a direct consequence of the value of *J* used in our calculations. There are also available experimental results from high-energy spectroscopy, which lead one to expect a value of $J=0.65\cdots 0.7$ eV (Ref. 75) instead of $J=0.8$ eV used in our calculation. We found that such a smaller value of *J* does not change our results significantly.

There is, however, an important part missing in our present calculation. Since we use the LDA DOS and not the full Hamiltonian in the DMFT caclulations, the a_{1g}-e_g^{π} *hybridization* is neglected completely. As has been pointed out by Anisimov *et al.*,[33] this hybridization can give rise to an antiferromagnetic Kondo coupling between a_{1g} and e_g^{π} orbitals and its value was estimated to be $J_K=-630$ K.[33] Thus, in LiV_2O_4 there are possibly three important exchange interactions present between the a_{1g} and e_g^{π} electrons of the V 3*d* shell: ferromagnetic double exchange (≈ 1090 K), antiferromagnetic direct exchange (≈ -450 K) and antiferromagnetic Kondo exchange [≈ -630 K (Ref. 33) not taken into account in our calculation]. All these interactions effectively cancel, eventually leading to a small Curie-Weiss temperature of the order of 0 K in accordance with experiment. Finally, one puzzle remains, namely, that the data from neutron scattering experiments show ferromagnetic spin fluctuations at high temperatures.[18,76]

The competing exchange terms described above may also explain the change from antiferromagnetic to ferromagnetic spin fluctuations at $T\approx 40$ K found in neutron scattering experiments. This is about the same energy scale as the coherence temperature of the Kondo lattice.[33] Thus, one might argue that, while below T_{coh} the combined antiferromagnetic direct and Kondo exchanges are stronger than the ferromagnetic double exchange, this changes above T_{coh} where the Kondo effect becomes ineffective, such that the ferromagnetic exchange prevails.

IV. CONCLUSION

We investigated the effect of Coulomb correlations on the electronic structure, orbital state and magnetic properties of LiV_2O_4. The analysis of the noninteracting partial densities of state obtained by standard LDA calculations shows that, while the trigonal splitting of the t_{2g} states into a_{1g} and e_g^{π} orbitals is not strong enough to produce separate bands, it leads to a significant difference in the effective bandwidths and average energy of the trigonal orbitals. The LDA +DMFT(QMC) calculations gave orbital occupancies and spectra which indicate a nearly complete localization of one electron out of 1.5 3*d* electrons per V ion in the a_{1g} orbital, while the e_g^{π} orbitals form a relatively broad partially filled metallic band. The calculated temperature dependence of the paramagnetic susceptibility corresponds to the experimentally observed Curie-Weiss law and gives an effective paramagnetic moment $p_{\text{eff}}=1.65$ in agreement with experimental data. The experimentally observed small value of the Curie-Weiss temperature, formerly a puzzle, is supposed to be the result of a competition between three different contributions to the effective exchange interaction between a_{1g} and e_g^{π} electrons in the V3*d* shell: ferromagnetic double exchange, antiferromagnetic direct exchange and antiferromagnetic Kondo exchange described in Ref. 33. The present calculations show a dominance of the first two exchanges. We suppose that including the hybridization between a_{1g} and e_g^{π} (next step of our research), can lead to an almost cancellation of all three exchanges and the experimentally observed small residual antiferromagnetic Curie-Weiss temperature might become possible.

ACKNOWLEDGMENTS

We thank A. Oles, A. Loidl, D. Singh, P. Horsch, and V. Eyert for very useful discussions, A. Sandvik for making available his maximum entropy program, and M. A. Korotin for supplying the unpublished results for LDA+U calculation. This work was supported in part by the Deutsche Forschungsgemeinschaft through Sonderforschungsbereich 484 (D.V., T.P., G.K., A.K., I.N.) and the Russian Foundation for Basic Research through Grants No. RFFI-01-02-17063 (V.A.,I.N.) and RFFI-02-02-06162 (IN).

[1] K. Andres, J.E. Graebner, and H.R. Ott, Phys. Rev. Lett. **35**, 1779 (1975).
[2] G.R. Stewart, Rev. Mod. Phys. **56**, 755 (1984).
[3] G. Aeppli and Z. Fisk, Comments Condens. Matter Phys. **16**, 155 (1992).
[4] S. Kondo, D.C. Johnston, C.A. Swenson, F. Borsa, A.V. Mahajan, L.L. Miller, T. Gu, A.I. Goldman, M.B. Maple, D.A. Gajewski, E.J. Freeman, N.R. Dilley, R.P. Dickey, J. Merrin, K. Kojima, G.M. Luke, Y.J. Uemura, O. Chmaissen, and J.D. Jorgensen, Phys. Rev. Lett. **78**, 3729 (1997).
[5] R. Ballou, E. Lelièvre-Berna, and B. Fak, Phys. Rev. Lett. **76**, 2125 (1996), and references therein.
[6] S.A. Carter, T.F. Rosenbaum, P. Metcalf, J.M. Honig, and J. Spalek, Phys. Rev. B **48**, 16 841 (1993).
[7] C. Urano, M. Nohara, S. Kondo, F. Sakai, H. Takagi, T. Shiraki, and T. Okubo, Phys. Rev. Lett. **85**, 1052 (2000).
[8] K. Kadowaki and S.B. Woods, Solid State Commun. **58**, 507 (1986).
[9] D.C. Johnston, C.A. Swenson, and S. Kondo, Phys. Rev. B **59**, 2627 (1999).
[10] T. Hayakawa, D. Shimada, and N. Tsuda, J. Phys. Soc. Jpn. **58**, 2867 (1989).
[11] S. Kondo, D.C. Johnston, and L.L. Miller, Phys. Rev. B **59**, 2609 (1999).
[12] M. Onoda, H. Imai, Y. Amako, and H. Nagasawa, Phys. Rev. B **56**, 3760 (1997).
[13] M. Lohmann, J. Hemberger, M. Nicklas, H.A. Krug von Nidda, A. Loidl, M. Klemm, G. Obermeier, and S. Horn, Physica B **259-261**, 963 (1999).
[14] A. Fujimori, K. Kawakami, and N. Tsuda, Phys. Rev. B **38**, 7889 (1988).
[15] N. Fujiwara, H. Yasuoka, and Y. Ueda, Phys. Rev. B **57**, 3539 (1998).
[16] N. Fujiwara, H. Yasuoka, and Y. Ueda, Phys. Rev. B **59**, 6294 (1999).
[17] A.V. Mahajan, R. Sala, E. Lee, F. Borsa, S. Kondo, and D.C. Johnston, Phys. Rev. B **57**, 8890 (2000).
[18] A. Krimmel, A. Loidl, M. Klemm, S. Horn, and H. Schober, Phys. Rev. Lett. **82**, 2919 (1999); Phys. Rev. B **61**, 12 578 (1998); Physica B **276-278**, 766 (2000).
[19] W. Trinkl and A. Loidl, M. Klemm, and S. Horn, Phys. Rev. B **62**, 8915 (2000).
[20] S.-H. Lee, Y. Qiu, C. Broholm, Y. Ueda, and J.J. Rush, Phys. Rev. Lett. **86**, 5554 (2001).
[21] K. Fujiwara, H. Yoshioka, K. Miyoshi, J. Takeuchi, T.C. Kobayashi, and K. Amaya, Physica B **312-313**, 913 (2002).
[22] D.C. Johnston, Physica B (to be published) cond-mat/9910404.
[23] F. Takagi, K. Kawakami, I. Maekawa, Y. Sakai, and N. Tsuda, J. Phys. Soc. Jpn. **56**, 444 (1987).
[24] Y. Nakajima, Y. Amamiya, K. Ohnishi, I. Terasaki, A. Maeda, and K. Uchinokura, Physica C **185-189**, 719 (1991).
[25] Y. Ueda, N. Fujiwara, and H. Yasuoka, J. Phys. Soc. Jpn. **66**, 778 (1997).
[26] H. Kessler and M.J. Sienko, J. Chem. Phys. **55**, 5414 (1971).
[27] B.L. Chamberland and T.A. Hewston, Solid State Commun. **58**, 693 (1986).
[28] M. Brando, N. Büttgen, V. Fritsch, J. Hemberger, H. Kaps, H.-A. Krug von Nidda, M. Nicklas, K. Pucher, W. Trinkl, A. Loidl, E.W. Scheidt, M. Klemm, and S. Horn, Eur. Phys. J. B **25**, 289 (2002).
[29] K. Miyoshi, M. Ihara, K. Fujiwara, and J. Takeuchi, Phys. Rev. B **65**, 092414 (2002).
[30] D. C. Johnston, T. Ami, F. Borsa, M. K. Crawford, J. A. Fernandez-Baca, K. H. Kim, R. L. Harlow, A. V. Mahajan, L. L. Miller, M. A. Subramanian, D. R. Torgeson, and Z. R. Wang, in *Spectroscopy of Mott Insulators and Correlated Metals*, edited by P. Fulde, Springer Ser. Solid-State Sci. Vol. 119 (Springer, Berlin, 1995), p. 20.
[31] W. Kohn, L.J. Sham, Phys. Rev. A **140**, 1133 (1965); L.J. Sham, W. Kohn, Phys. Rev. **145**, 561 (1966).
[32] L. Hedin and B. Lunqvist, J. Phys. C **4**, 2064 (1971); U. von Barth and L. Hedin, *ibid.* **5**, 1629 (1972).
[33] V.I. Anisimov, M.A. Korotin, M. Zölfl, T. Pruschke, K. Le Hur, and T.M. Rice, Phys. Rev. Lett. **83**, 364 (1999).
[34] O.K. Andersen, Phys. Rev. B **12**, 3060 (1975); O. Gunnarsson, O. Jepsen, and O.K. Andersen, *ibid.* **27**, 7144 (1983).
[35] V.I. Anisimov, J. Zaanen, and O.K. Andersen, Phys. Rev. B **44**, 943 (1991); J. Phys.: Condens. Matter **9**, 767 (1997).
[36] V. Eyert, K.-H. Höck, S. Horn, A. Loidl, and P.S. Riseborough, Europhys. Lett. **46**, 762 (1999).
[37] A.R. Williams, J. Kübler, and C.D. Gellat, Jr., Phys. Rev. B **19**, 6094 (1979).
[38] J. Matsuno, A. Fujimori, and L.F. Mattheiss, Phys. Rev. B **60**, 1607 (1999).
[39] L.F. Mattheiss and D.R. Hamann, Phys. Rev. B **33**, 823 (1986).
[40] O.K. Andersen, Phys. Rev. B **12**, 3060 (1975).
[41] L.F. Mattheiss and W. Weber, Phys. Rev. B **25**, 2248 (1982).
[42] D.J. Singh, P. Blaha, K. Schwarz, and I.I. Mazin, Phys. Rev. B **60**, 16 359 (1999).
[43] D.J. Singh, *Planewaves, Pseudopotentials and the LAPW Method* (Kluwer Academic, Boston, 1994).
[44] P. Blaha, K. Schwartz, and J. Luitz, Vienna University of Technology, 1997 [Improved and updated Unix version of the WIEN code, published by P. Blaha, K. Schwartz, P. Sorantin, and S.B. Trickey, Comput. Phys. Commun. **59**, 399 (1990)].
[45] S.H. Wei and H. Krakauer, Phys. Rev. Lett. **55**, 1200 (1985); D. Singh, Phys. Rev. B **43**, 6388 (1991).
[46] C.M. Varma, Phys. Rev. B **60**, R6973 (1999).

[47] H. Kusunose, S. Yotsuhashi, and K. Miyake, Phys. Rev. B **62**, 4403 (2000).
[48] J. Hopkinson and P. Coleman, Phys. Rev. Lett. **89**, 267201 (2002).
[49] J. Hopkinson and P. Coleman, Physica B **312**, 711 (2002).
[50] S. Fujimoto, Phys. Rev. B **65**, 155108 (2002).
[51] S. Burdin, D.R. Grempel, and A. Georges, Phys. Rev. B **66**, 045111 (2002).
[52] B. Reuter and J. Jaskowsky, Angew. Chem. **72**, 209 (1960).
[53] H. Wada, M. Shiga, and Y. Nakamura, Physica B **161**, 197 (1989).
[54] O. Chmaissem and J.D. Jorgensen, S. Kondo, and D.C. Johnston, Phys. Rev. Lett. **79**, 4866 (1997).
[55] V. Eyert and K.-H. Höck, Phys. Rev. B **57**, 12 727 (1998).
[56] K. Terakura, T. Oguchi, A.R. Williams, and J. Kübler, Phys. Rev. B **30**, 4734 (1984).
[57] W. Metzner and D. Vollhardt, Phys. Rev. Lett. **62**, 324 (1989).
[58] D. Vollhardt, in *Correlated Electron Systems*, edited by V. J. Emery (World Scientific, Singapore, 1993), p. 57.
[59] Th. Pruschke, M. Jarrell, and J. K. Freericks, Adv. Phys. **44**, 187 (1995).
[60] A. Georges, G. Kotliar, W. Krauth, and M. J. Rozenberg, Rev. Mod. Phys. **68**, 13 (1996).
[61] V. I. Anisimov, A. I. Poteryaev, M. A. Korotin, A. O. Anokhin, and G. Kotliar, J. Phys.: Condens. Matter **9**, 7359 (1997).
[62] A. Lichtenstein and M. I. Katsnelson, Phys. Rev. B **57**, 6884 (1998).
[63] K. Held, I.A. Nekrasov, N. Blümer, V.I. Anisimov, and D. Vollhardt, Int. J. Mod. Phys. B **15**, 2611 (2001); K. Held, I.A. Nekrasov, G. Keller, V. Eyert, N. Blümer, A.K. McMahan, R.T. Scalettar, T. Pruschke, V.I. Anisimov, and D. Vollhardt, in *Quantum Simulations of Complex Many-Body Systems: From Theory to Algorithms*, edited by J. Grotendorst, D. Marks, and A. Muramatsu, NIC Series Volume 10 (NIC Directors, Forschunszentrum Jülich, 2002), p. 175–209.
[64] J.E. Hirsch and R.M. Fye, Phys. Rev. Lett. **56**, 2521 (1986); M. Jarrell, *ibid.* **69**, 168 (1992); M. Rozenberg, X. Y. Zhang, and G. Kotliar, *ibid.* **69**, 1236 (1992); A. Georges and W. Krauth, *ibid.* **69**, 1240 (1992); M. Jarrell in *Numerical Methods for Lattice Quantum Many-Body Problems*, edited by D. Scalapino (Addison Wesley, New York, 1997). For review of QMC for DMFT see Ref. 63.
[65] For a review on the maximum entropy method see M. Jarrell and J.E. Gubernatis, Phys. Rep. **269**, 133 (1996).
[66] I.A. Nekrasov, K. Held, N. Blümer, A.I. Poteryaev, V.I. Anisimov, and D. Vollhardt, Eur. Phys. J. B **18**, 55 (2000).
[67] M. A. Korotin (unpublished).
[68] K. Held, G. Keller, V. Eyert, D. Vollhardt, and V.I. Anisimov, Phys. Rev. Lett. **86**, 5345 (2001).
[69] M. B. Zölfl, Th. Pruschke, J. Keller, A.I. Poteryaev, I.A. Nekrasov, and V.I. Anisimov, Phys. Rev. B **61**, 12 810 (2000).
[70] A. Liebsch and A. Lichtenstein, Phys. Rev. Lett. **84**, 1591 (2000).
[71] Ph. Lambin and J.P. Vigneron, Phys. Rev. B **29**, 3430 (1984).
[72] O. Gunnarsson, O.K. Andersen, O. Jepsen, and J. Zaanen, Phys. Rev. B **39**, 1708 (1989); V.I. Anisimov and O. Gunnarsson, *ibid.* **43**, 7570 (1991).
[73] Recently the Curie-Weiss law was derived analitically in dynamical mean-field theory for the Hubbard model [K. Byczuk and D. Vollhardt, Phys. Rev. B **65**, 134433 (2002)].
[74] Experimental data were interpreted as a sum of Pauli and Curie-Weiss paramagnetic contributions to the susceptibility (Ref. 17). However, for high temperatures the dominant contribution is of Curie-Weiss type. As DMFT calculations were done for very high temperatures (1000 K and more), we neglected Pauli contribution in our analysis of calculated data.
[75] J. Zaanen and G. A. Sawatzky extracted the value of $J = 0.64$ eV obtained from Racah parameters for V ions [J. Solid State Chem. **88**, 8 (1990)] using the procedure, described in J. S. Griffith, *The Theory of Transition Metal Ions* (Cambridge University Press, Cambridge, 1971). T. Mizokawa and A. Fujimori deduced from the cluster-model analyses of the photoemission spectra $J = 0.68$ eV [Phys. Rev. B **54**, 5368 (1996)].
[76] A. Krimmel, A. P. Murani, J. R. Stewart, A. Ibarra-Palos, P. Strobel, and A. Loidl, Acta Phys. Pol. (to be published).